Acta Materialia 199 (2020) 1–8

Contents lists available at ScienceDirect

Acta Materialia

journal homepage: www.elsevier.com/locate/actamat

Full length article

Icosahedral and dodecagonal quasicrystal plus glass alloys with plastic deformability

Y. Jin[a], A. Inoue[a,b,c,d,e,*], F.L. Kong[b], S.L. Zhu[a], F. Al-Marzouki[d], A.L. Greer[f]

[a] School of Materials Science and Engineering, Tianjin University, Tianjin 300072, China
[b] International Institute of Green Materials, Josai International University, Togane 283-8555, Japan
[c] School of Materials Science and Engineering, China University of Mining Technology, Xuzhou 221116, China
[d] Department of Physics, King Abdulaziz University, Jeddah 22254, Saudi Arabia
[e] MISiS, National University of Science and Technology, Moscow 119049, Russia
[f] Department of Materials Science and Metallurgy, University of Cambridge, Cambridge CB3 0FS, UK

ARTICLE INFO

Article history:
Received 13 March 2020
Revised 3 August 2020
Accepted 7 August 2020
Available online 12 August 2020

Keywords:
Quasicrystals
Plasticity
Hardness
Shear bands

ABSTRACT

Glassy ribbons of $Zr_{65}Al_{7.5}Ni_{10}Cu_{17.5-x}Au_x$ (x = 6–17.5 at%), cold-rolled at liquid-nitrogen temperature, transform into glass and icosahedral quasicrystalline [glass' + (IQ)] or [glass' + IQ + dodecagonal quasicrystalline (DoQ) + approximant crystalline (APC)] phases. The rolled ribbons show plasticity, an unprecedented contrast to the extreme brittleness of all alloys containing large size IQ-, DoQ- and APC particles reported to date. After thickness reductions (R) of 50–70%, the structure is [glass' + IQ] for 6–15Au and [glass' + IQ + DoQ + APC] phases for 17.5Au. The IQ and DoQ particle diameters are 50–100 nm and 150–200 nm, respectively, much larger than the 10–15 nm for the IQ phase when induced by annealing. On cold-rolling, the Vickers hardness decreases by up to 24% at R = 70%, in contrast to the hardening effect of annealing-induced transformation. Tensile tests on cold-rolled ribbons show evidence for preferential slip at pre-existing shear bands. The rolling-induced quasicrystalline phases have quasiperiodic atomic arrangements that are incompletely developed and do not extend over long range; the high density of internal defects and strains appears to promote plasticity. The success in synthesizing plastic [glass' + IQ] and [glass' + DoQ + APC] alloys may provide a new method for ductilization of brittle materials, and is promising for the development of a new type of structural material.

1. Introduction

Metallic materials consist of up to three types of phases with crystalline, glassy (amorphous), or quasicrystalline atomic configurations. The first synthesis of a metallic glass by rapid solidification was for an Au-Si alloy in 1960 [1], while the icosahedral quasicrystalline (IQ) phase was discovered in a rapidly solidified $Al_{86}Mn_{14}$ (at%) alloy in 1984 [2]. At present, metallic glasses can be cast in bulk form with maximum diameter above 1 cm in a wide variety of alloy systems, and they possess several properties that are attractive compared to their crystalline counterparts [3–6], e.g. higher strength, elastic strain, electrical resistivity, thermal expansion coefficient, surface smoothness, optical reflectivity, corrosion resistance, viscous deformability, and also net-shape castability due to the much smaller shrinkage during solidification. Bulk-glass-forming compositions: (1) are multicomponent, consisting of three elements or more; (2) have significant mismatches (> 12%) in the atomic radii of the three main elements; and (3) have negative heats of mixing between the main constituent elements [6–8]. Fe-based and Zr-based bulk metallic glasses (BMGs) have found application as soft-magnetic, sensor, micro-machinery, casing, spring, hinge, biomedical screw, sporting goods, structural and surface coating materials [6–8]. On the other hand, IQ alloys show very high hardness, high wear resistance and electrical resistivity, and low thermal conductivity in comparison with conventional crystalline alloys [9–11]. Although these properties of IQ alloys may be attractive, their ultra-high brittleness has precluded their development as practical engineering materials. This brittleness is thought to originate from the difficulty of dislocation movement in the quasiperiodic lattice and from the strong covalent nature of the bonding between their constituent elements [9–11].

The strength and plasticity of as-cast Zr-based BMGs decrease significantly in systems containing IQ particles [12], though the

* Corresponding author at: School of Materials Science and Engineering, Tianjin University, Tianjin 300072, China.
E-mail addresses: inoue@jiu.ac.jp (A. Inoue), slzhu@tju.edu.cn (S.L. Zhu), alg13@cam.ac.uk (A.L. Greer).

https://doi.org/10.1016/j.actamat.2020.08.009

compressive deformation-induced formation of a nanocluster IQ region along the shear bands leads to an increase of ductility [13,14]. The homogeneous dispersion of nanoscale IQ phase is obtained by annealing-induced partial transformation of Zr-Al-Ni-Cu-M glasses containing elements with positive heats of mixing and/or large atomic size mismatch such as M = Ag, Pd, Pt, Au or Nb [15–19]. Besides, high-pressure torsion has been applied to $Zr_{65}Al_{10}Ni_{10}Cu_{17}Au_3$ glasses, and the deformed alloys show higher H_V and smaller heats of crystallization with increasing the number of torsion cycles, accompanying the precipitation of nanoscale metastable cubic Zr_2Ni compound with a particle diameter of 5–7 nm, which is distinct from IQ and APC phases [20]. However, increases in the volume fraction and particle size of IQ phase caused a drastic decrease in plasticity and a significant decrease in fracture strength [12,15–18]. To date, there have been no data on the synthesis of plastic IQ-containing glass alloys with large particle size above several tens of nanometers. If a glassy alloy containing large particle size IQ phase with plasticity could be synthesized, this would mark a third kind of plastic metallic material, in addition to crystalline and glassy alloys. Such a breakthrough would require a fundamental revision of the current concept of brittle quasilattice metallic materials.

We recently reported that cold-rolling of Al-Y and Al-Y-Ni-Co amorphous alloys can induce a novel transformation mode [21]. The rolling-induced precipitate is an fcc-Al supersaturated solid solution with the same nominal composition as the alloy, implying formation by polymorphic crystallization, i.e. without appreciable redistribution of the constituent elements. This is completely different from the annealing-induced crystallization of Al-Ln (Ln = lanthanide metal) and Al-Ln-Ni-Co glasses, which gives [fcc-Al + compound] phases with compositions significantly different from the amorphous matrix [22–25]. In addition, the cold-rolled Al-based alloys with [fcc-Al supersaturated solid solution + residual amorphous] phases retain good bending plasticity in conjunction with a distinct decrease in hardness [21], in contrast to the loss of bending plasticity and significant increase in hardness for annealing-induced crystallization of the same Al-based alloys [22,23]. The significantly different structure, transformation behavior and mechanical properties, arising from the cold-rolling, suggest that this can be regarded as a useful method for synthesis of a novel and potentially useful metastable phases.

The present work reports that glassy alloys containing large particle sizes of IQ phase, or a mixture of [IQ + dodecagonal quasicrystalline (DoQ) + approximant crystalline (APC)] phases, in each case with good bending plasticity, can be formed by cold-rolling of $Zr_{65}Al_{7.5}Ni_{10}Cu_{17.5-x}Au_x$ (x = 6–17.5 at%) and Zr-Al-Ni-Au glasses. This is the first evidence for the synthesis of large particle size IQ- and [IQ + DoQ + APC]-containing glass alloys with good plasticity, and provides the first insight on the effects of cold-rolling on IQ, DoQ and APC atomic configurations. There are opportunities to clarify the structural relationship among the IQ, DoQ and glassy phases, and the processes by which they are formed. We characterize the microstructure, mechanical properties and thermal stability of the rolling-induced IQ- and [IQ + DoQ + APC]-containing glass alloys, and assess the usefulness of cold-rolling to synthesize new useful metastable phases in such systems.

2. Experimental methods

Multicomponent Zr-based alloys with nominal compositions $Zr_{65}Al_{7.5}Ni_{10}Cu_{17.5-x}Au_x$ (x = 6, 10, 15 and 17.5 at%) were chosen because this alloy series forms bulk glasses that can crystallize to give a mixture of [glass' + IQ] phases [15]. The alloy ingots were prepared by arc-melting the mixtures of pure metals with purities above 99.9 wt% under an argon atmosphere. Ribbons with thickness ≈ 30–40 μm and width ≈ 2 mm were prepared by single-roller melt-spinning; the circumferential velocity of the copper wheel was ~ 30–37 m s^{-1}. The amorphicity of the samples was confirmed by X-ray diffraction (XRD) and transmission electron microscopy (TEM). Thermal stability associated with the glass transition, supercooled-liquid region and crystallization was examined by differential scanning calorimetry (DSC) with a heating rate of 0.67 K s^{-1}. For cold-rolling, the ribbons were sandwiched between two type-304 stainless-steel plates, each with an initial thickness of 2 mm. The sandwich structures were passed through a twin-roller machine to obtain a thickness reduction of ~5% in each pass. Several dozen passes were used to obtain ribbons with total thickness reductions in the range up to ~70%. Rolling was conducted mostly close to liquid-nitrogen temperature (LNT, near 77 K); for this, the sandwich structure was immersed in liquid nitrogen for 600 s before being taken out and immediately rolled. The initial Vickers hardness of the stainless-steel sheet was 270, and this ultimately rose to ~600 as a result of the rolling. The tensile stress-strain curve was measured for the as-spun and cold-rolled ribbons at room temperature (RT) using an Instron testing machine. The gauge dimension was ~2 mm in width and ~10 mm in length. The initial strain rate was 8.3×10^{-5} s^{-1}. The structure of the cold-rolled ribbons was examined by XRD, scanning electron microscopy (SEM), standard TEM and high-resolution TEM (HRTEM) (JEOL-300, FEI Tecnai F30) equipped with nanobeam electron diffraction and EDX spectroscopy. The thin foils for TEM observation were prepared at liquid nitrogen temperature under very mild milling conditions with a 3 keV, 40 μA beam at a grazing incidence angle of 3 degrees. It is further confirmed that no crystalline phase is recognized in the as-spun 10Au alloy ribbon with a thin foil made under the same milling conditions. The bending plasticity was evaluated by a simple bend test; ribbons that can be bent through 180° and then back to the original straight condition are considered to be "plastic". The tensile fracture surface and the bent outer surface were examined by SEM.

3. Results

Fig. 1a, b show XRD patterns and DSC curves of melt-spun $Zr_{65}Al_{7.5}Ni_{10}Cu_{17.5-x}Au_x$ (x = 6–17.5 at%) ribbons. The ribbons exhibit only broad haloes in the XRD patterns with no detectable crystalline peaks. The DSC traces show the glass transition, followed by the supercooled-liquid region and then two exotherms, indicating that crystallization proceeds through two stages. The XRD patterns of the 6–17.5Au ribbons annealed for 1800 s at a temperature above the first exotherm can be identified as [glass' + IQ] phases (Fig. 1c). Fig. 1d,e show a bright-field TEM image and selected-area electron diffraction pattern of the 10Au ribbon annealed for 1800 s at 761 K; annealing gives spheroidal particles of an IQ phase, with diameter as small as 10–15 nm, dispersed in a glassy matrix. These annealed ribbons are very brittle, and fracture easily during bending, being consistent with the previous findings that the annealing-induced IQ-based alloys for Pd-U-Si, Al-Cu-V, Al-Mn-Si amorphous systems are very brittle [26–29].

Fig. 2 shows bright-field TEM images and selected-area electron diffraction patterns of the 10Au (a, b) and 17.5Au (c, d) alloys cold-rolled to about 70% reduction in thickness at LNT. The precipitates in the 10Au ribbon have a diameter of about 100 nm and occupy an area fraction estimated to be as high as 70%. The thin foil thickness used for the TEM observation with a 300 keV acceleration voltage electron microscope is presumed to be 250–300 nm [30]. This is greater than average diameter (~75 nm) of the IQ particles. We take the ratio of foil thickness to particle diameter to be a good estimate of the ratio of area to volume fractions. On this basis, the volume fraction of the IQ phase is estimated to be 18–21 %. The diffraction pattern from one of the precipitates shows five-fold symmetry, indicating that the precipitates

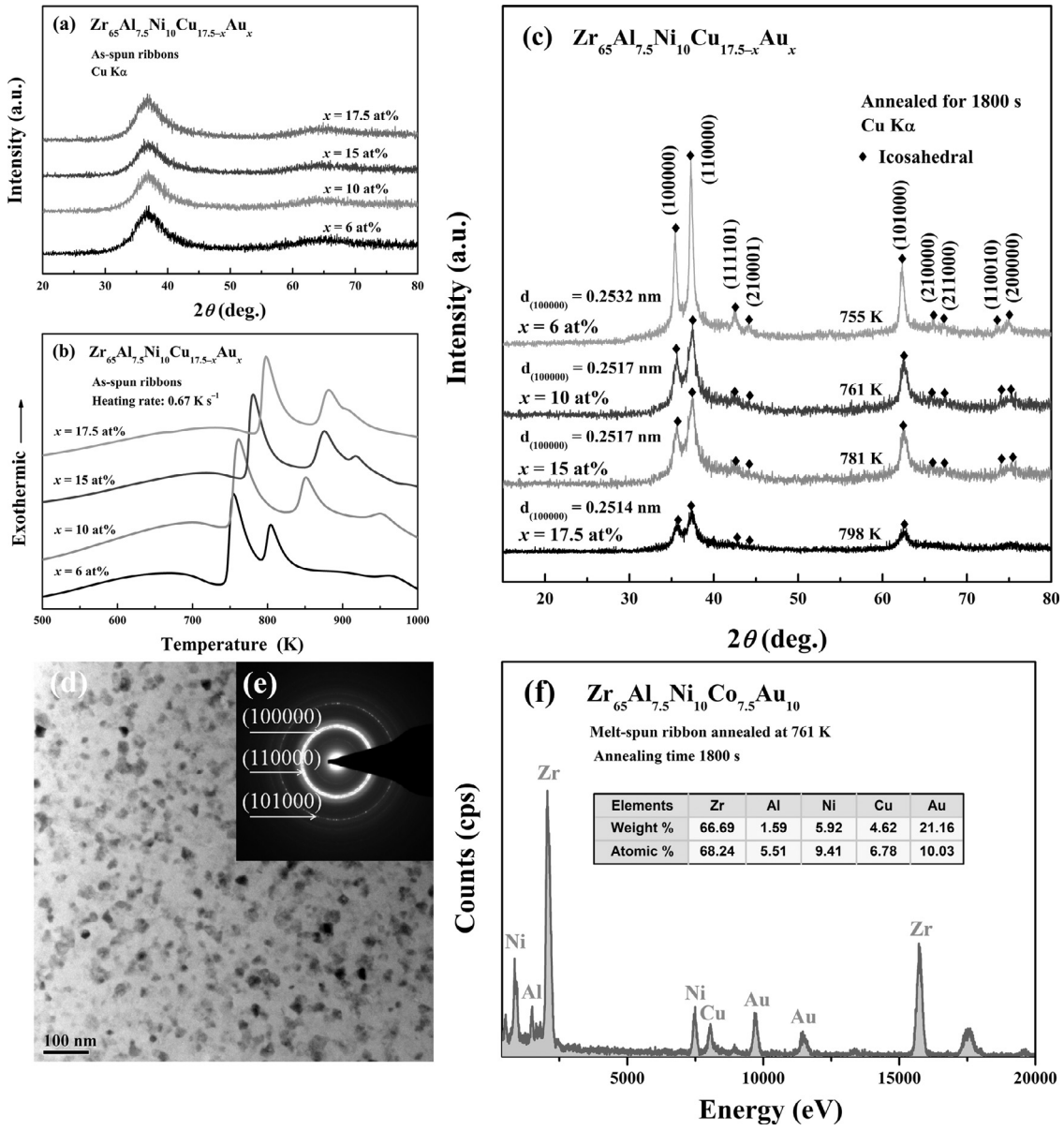

Fig. 1. (a) X-ray diffraction patterns and (b) DSC curves, of as-spun $Zr_{65}Al_{7.5}Ni_{10}Cu_{17.5-x}Au_x$ (x = 6–17.5 at%) glassy ribbons. (c) X-ray diffraction patterns of the 6–17.5% Au glassy alloys annealed for 1.8 ks at a temperature just above the first exotherm. For the 10Au alloy annealed for 1.8 ks at 761 K: (d) bright-field TEM image, (e) selected-area electron diffraction pattern, and (f) energy-dispersive X-ray (EDX) spectroscopy profiles taken from an IQ-phase region.

are an IQ phase. This phase includes a high density of internal defects as marked with arrows. The selected-area electron diffraction patterns of the IQ phase region are shown in Fig. 2e. On the other hand, the region "A" in the 17.5Au alloy contains a high density of plane faults and the selected-area electron diffraction pattern (Fig. 2f) taken from the region is identified as an approximant crystalline (APC) phase with a much larger lattice parameter of about 0.72 nm, roughly three times the lattice spacing (a_q = 0.251 nm) for the (110,000) plane of the IQ phase. A number of streaks are observed along the <110,000> and <100,000> directions, indicating that planar faults lie along the (110,000) and (100,000) planes. The close correlation between the APC phase and the IQ phase implies that the APC phase with a cubic structure of a lattice parameter of 0.75 nm, which can be regarded as a stoichiometric Zr_2(Al, Ni, Cu, Au) phase, was formed by strain-induced transformation. Many distinct streaks (marked with arrows) in the electron diffraction pattern for the APC phase indicate that high levels of strains and distortions co-exist with the planar faults. There is little evidence for the residual amorphous phase in the bright-field TEM image or the selected-area electron diffraction pattern (Fig. 2c–f).

Fig. 3 shows HRTEM images and nanobeam diffraction patterns of the rolling-induced IQ phase in the 10Au (a, b) alloy and dodecahedral quasicrystalline (DoQ) phase in the 17.5Au (c, d) alloy, in comparison with the annealing-induced IQ phase in the 10Au alloy (e, f). The HRTEM of icosahedral atomic configurations shows a regular arrangement over a long range for the annealing-induced phase, but over a much shorter range in the cold-rolled ribbons (Fig. 3a, c). The selected-area electron diffraction patterns (b) and (d) show five-fold and twelve-fold symmetries, respectively, indicating the formations of IQ and DoQ phases. The HRTEM image from the DoQ phase reveals an irregular periodic atomic arrangement including a number of misfitting regions, indicating that the DoQ phase also includes a high density of defects, consistent with the generation of the streaks in the electron diffraction pattern of APC phase shown in Fig. 2f. Overall it is clear that the rolling-induced IQ, DoQ and APC phases contain a high density of inter-

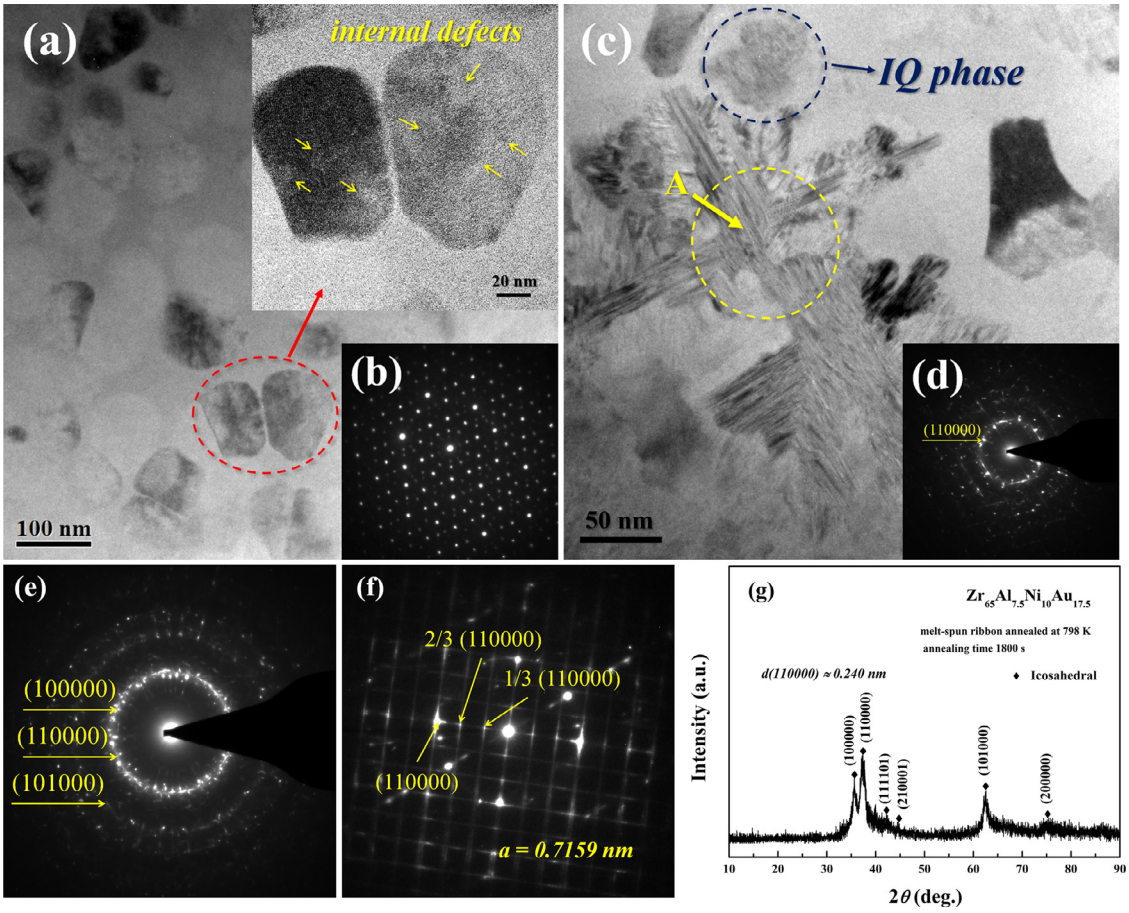

Fig. 2. Bright-field TEM images and selected-area electron diffraction (SAED) patterns of $Zr_{65}Al_{7.5}Ni_{10}Cu_{17.5-x}Au_x$ with x = 10 (a, b) and x = 17.5 at% (c, d) alloy ribbons cold-rolled to about 70% reduction in thickness (R), respectively; SAED patterns taken from the region of IQ phase (e) and "A" (f) in Fig. 2(c); (g) X-ray diffractogram of an 17.5Au alloy ribbon annealed for 1.8 ks at 798 K (shown for reference).

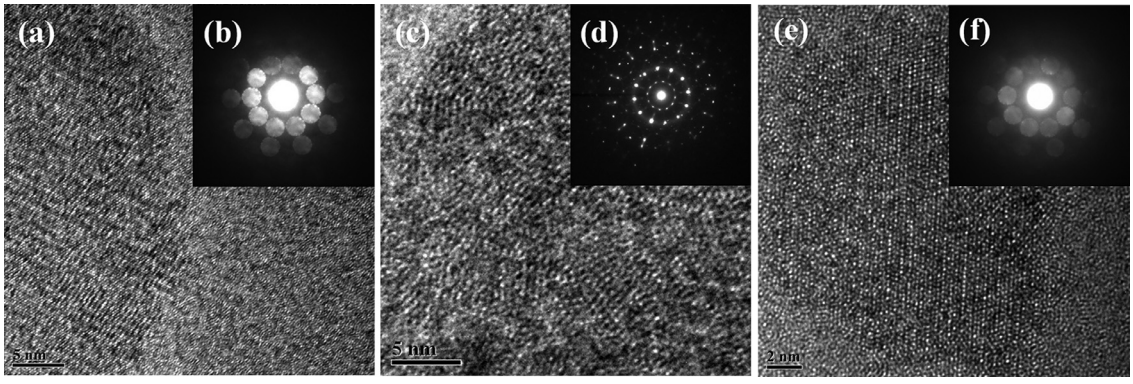

Fig. 3. High-resolution TEM images and nanobeam diffraction patterns of $Zr_{65}Al_{7.5}Ni_{10}Cu_{17.5-x}Au_x$ ribbons cold-rolled to $R \approx 70\%$: (a, b) for 10Au, and (c, d) for 17.5Au. For comparison, (e, f) an image and diffraction pattern for the 10Au ribbon annealed for 1.8 ks at 761 K.

nal defects and strains that make them quite distinct from the annealing-induced IQ phase. The high density of defects prevents the formation of well-developed icosahedral atomic configurations over long range.

Although a twelve-fold DoQ phase has been reported in rapidly solidified $V_{15}Ni_{10}Si$ [31], evaporated $BiMn_3$ thin film [32], fully annealed $Ta_{62}Te_{38}$ alloy [33] and rapidly solidified $Al_{65}Cu_{25}Fe_5V_5$ [34], there is no report on the formation of Zr-based alloys with twelve-fold symmetry in rapidly solidified and annealing-induced crystallization states, indicating that cold-rolling of a glass is a novel method to synthesize a new metastable phase.

Fig. 4 shows the changes in the DSC curves and XRD patterns induced by cold-rolling of $Zr_{65}Al_{7.5}Ni_{10}Cu_{17.5-x}Au_x$ (x = 10, 15 and 17.5 at%) ribbons. The 10Au cold-rolled ribbon shows a reduced heat for the first exotherm indicating the progress of quasicrystallization. The reduction of the first exothermic heat is calculated to be about 19% for the 10Au alloy cold-rolled to ~70%. Here, it is important to note that deformation induces a highly defected IQ structure, transformation to which releases less enthalpy than transformation of the same volume fraction by heating. For this reason, the relative difference in ΔH of the first peak in the DSC traces (Fig. 4a) does not scale exactly with the volume fraction of

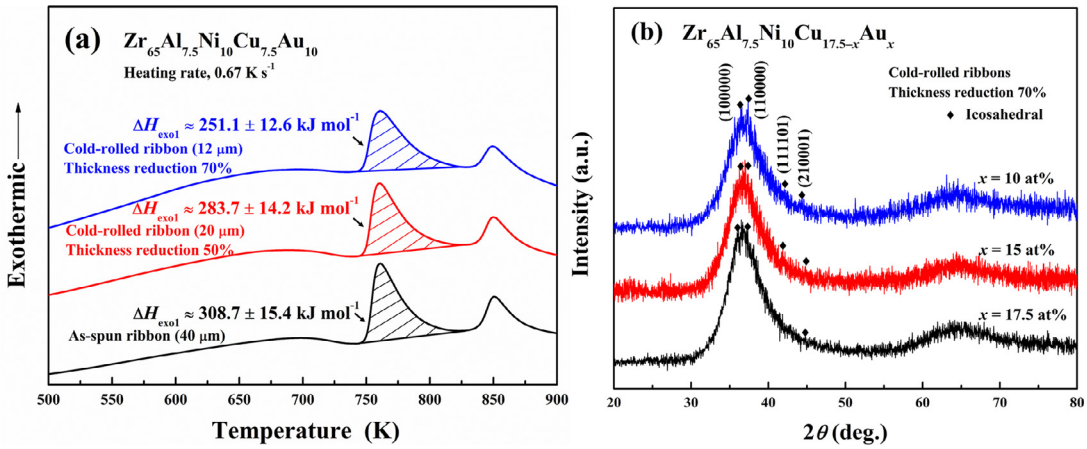

Fig. 4. (a) DSC curves of the as-spun and cold-rolled (thickness reduction R = 50% and 70%) 10Au ribbons. (b) X-ray diffraction patterns of the 10, 15 and 17.5 at% Au ribbons cold-rolled to $R \approx 70\%$.

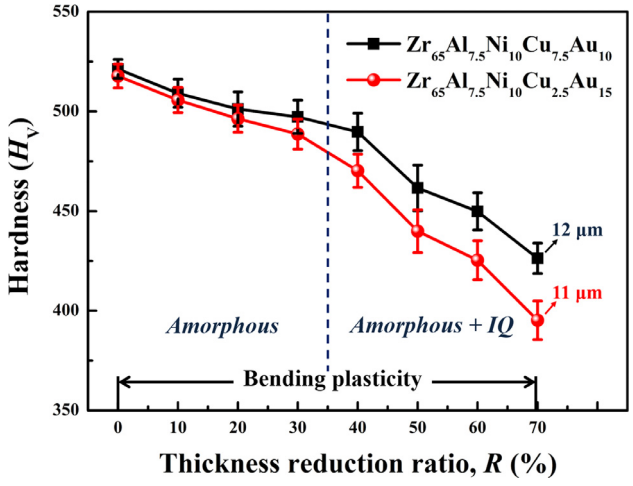

Fig. 5. Changes in structure, Vickers hardness (H_V) and bending plasticity as a function of the reduction in thickness R on cold-rolling $Zr_{65}Al_{7.5}Ni_{10}Cu_{17.5-x}Au_x$ (x = 10 and 15 at%) glassy ribbons. The final ribbon thicknesses are noted.

rolling-induced IQ phase; this volume fraction cannot be accurately determined only from the DSC data. In particular, the volume fraction of IQ phase induced by thickness reduction of 70% is thought to be somewhat larger than 19% indicated by the reduction of the first exothermic heat. Overall, the TEM images and DSC data allow for a consistent interpretation of the fraction transformed.

On the other hand, no change is found in the second exotherm. The XRD patterns of the glasses after cold-rolling to $R \approx 70\%$ show the broad glassy-phase halo and some small peaks corresponding to the main reflections of IQ phase and indicating its precipitation in the cold-rolled ribbons. However, the diffraction peak intensity of IQ phase is much lower for cold-rolled than for annealed ribbons. A similar significant difference in diffraction peak intensity is found between the cold-rolled and annealed Al-based glasses [21]. The much lower intensity for the IQ phase in the former case is attributed to the high density of internal defects and high levels of strains and distortions caused by repeated cold-rolling.

We further examined the changes in the structure, Vickers hardness (H_V) and bending plasticity with cold-rolling reduction in thickness R for the 10Au and 15Au glasses. As shown in Fig. 5, H_V shows a continuous decrease with increasing R from ~520 in the as-spun state to 430 for 10Au alloy and 395 for 15Au alloy after rolling to R = 70%. The decrease in H_V appears to change at $R \approx 40\%$ where the rolled structure changes from the glass to the mixed [glass' + IQ] phase. Annealing the 10Au alloy leads to precipitation of IQ phase and H_V values that increase significantly with annealing temperature [20]. The present decrease in H_V found on rolling is thus completely opposite to the previous result. Here it is notable that the good bending plasticity is maintained for all the cold-rolled ribbons. This is in contrast to all the previous data [26–29,31,35] that IQ and APC phase alloys are extremely brittle. This discovery that IQ- and [IQ + DoQ + APC]-based alloys can be ductilized by cold-rolling is extremely important for future structural and functional applications of such alloys.

SEM images of the outer bent surfaces of 15Au and 17.5Au ribbons in as-spun and R ≈ 70% states, are shown in Fig. 6a–f, together with the outer surface photo of the cold rolled ribbon sample subjected to bending (e). No change is seen with Au content: in each case there are several deformation bands without appreciable cracking. This result indicates that the rolling-induced IQ- and [IQ + DoQ + APC] phases with rather large particle diameters of 50–200 nm surrounded by the residual glassy phase have good plastic deformability at RT and LNT.

Fig. 7a shows the tensile stress-strain curve of the 10Au ribbon consisting of [glass' + IQ] phases obtained by cold-rolling to ~70%, together with that of the as-spun ribbon. Although the fracture strength of the rolled ribbon is rather low (~430 MPa), the stress-strain curve, even within this nominally elastic regime, includes a number of serrations that seem to originate from further localized slip at the rolling-induced deformation bands. On the other hand, no distinct serrated flow is seen for the as-spun glassy ribbon, for which the stress-strain curve has the form generally seen for metallic glasses.

The tensile fracture surface of the cold-rolled ribbon consists of smooth and vein-pattern regions, as shown in Fig. 7b. Although this combination is the same as for as-spun ribbon, the smooth region occupies >50% of the total fracture cross-section, compared to <20% for ordinary as-spun glassy ribbons. This significant difference may reflect the ease of subsequent sliding on the rolling-induced pre-existing shear bands. This behavior is also consistent with the serrated flow seen in the tensile stress-strain curve for the rolled ribbon.

4. Discussion

As shown in Figs. 1 and 2, the particle size of the IQ phase is 10–15 nm for the annealed alloys and 50–100 nm for the cold-rolled alloys. The significant difference implies that the ratio of nucleation frequency to growth rate is much lower for the IQ phase when it is induced by cold-rolling. A low nucleation frequency may

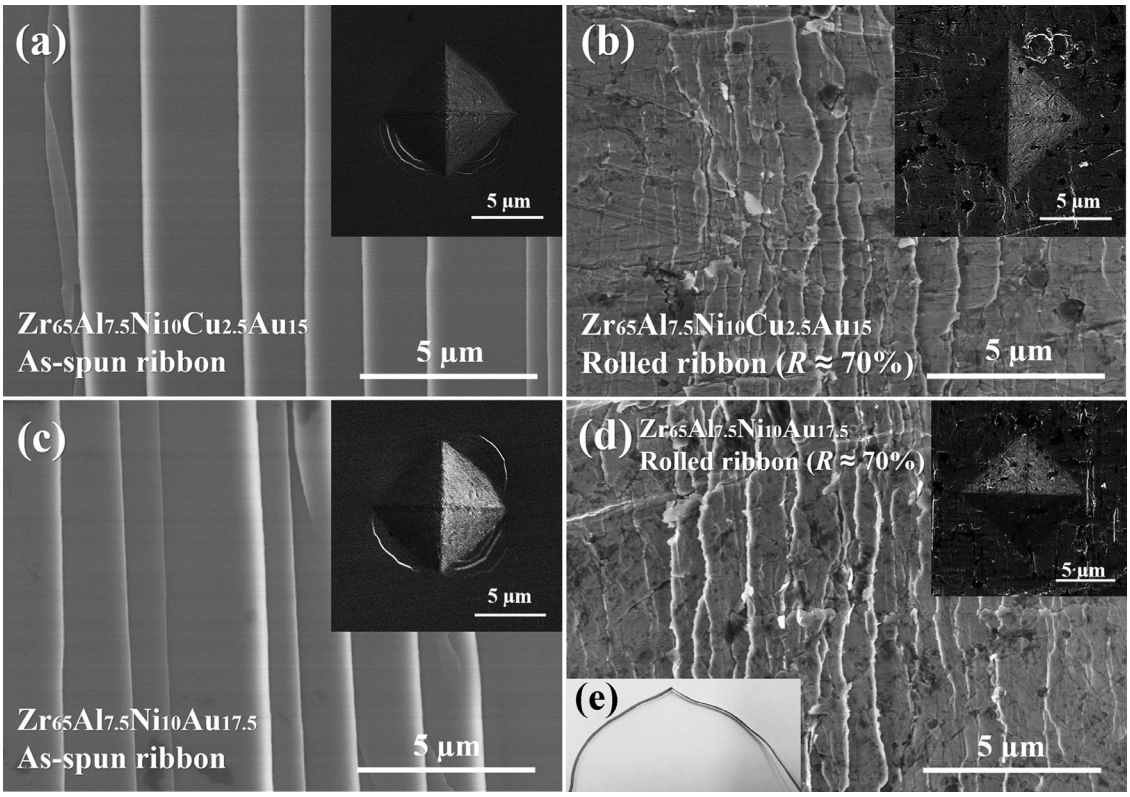

Fig. 6. SEM images of the outer surface of bent ribbons, and (inset) optical micrographs of Vickers hardness indents in,$Zr_{65}Al_{7.5}Ni_{10}Cu_{17.5-x}Au_x$ ribbons: (a) 15Au, as-spun, (b) 15Au, $R \approx 70\%$, (c) 17.5Au, as-spun, (d) 17.5Au, $R \approx 70\%$, (e) the outer surface photo of the cold rolled ribbon sample subjected to bending.

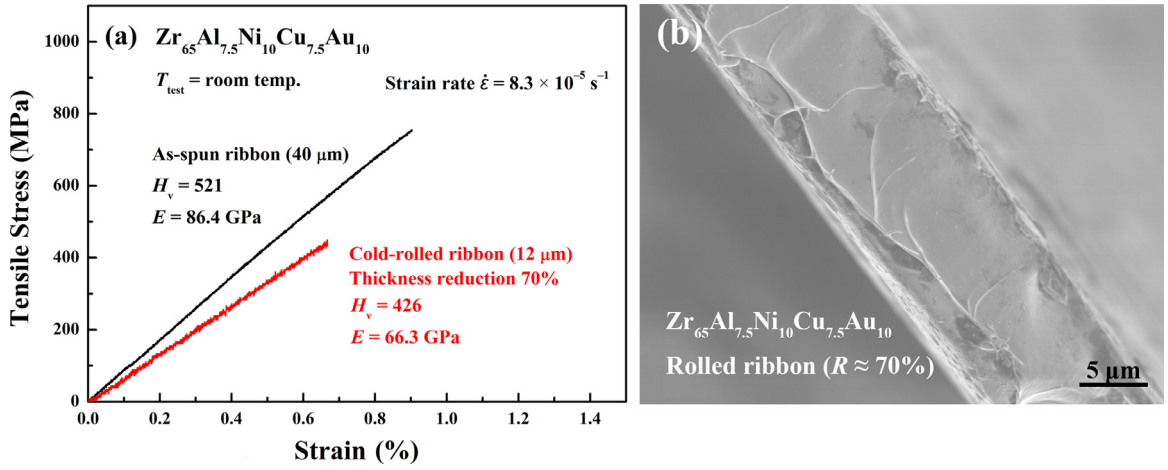

Fig. 7. (a) Tensile stress-strain curves at RT for as-spun glassy and cold-rolled IQ-based 10Au ribbons, and (b) SEM images of the fracture surface.

be due to the limited number of nucleation sites in the highly localized shear-band regions. On the other hand, the higher growth rate is presumably because the resulting IQ phase has incomplete quasiperiodic order over a long scale caused by the inclusion of internal defects and distortions. This is in contrast to the experimental evidence from the much smaller diameter of annealing-induced IQ particles, resulting from the difficulty of atomic diffusivity in the multicomponent alloys. The rolling-induced formation of the IQ phase may also be aided by adiabatic heating in the limited local shear-band regions, where the temperature can rise to a few thousand kelvins instantaneously, enhancing the atomic mobility [36–39]. It is presumed that the repeated temperature rises caused by the sequential rolling can enable the precipitation of highly defected IQ phase with much larger particle size.

Fig. 8 shows a schematic thermodynamic description of quasi-crystallization for the 17.5Au alloy. Here, the alloy is treated as binary with all solutes considered together. The free energies of the equilibrium ZrM, Zr_4M_3, Zr_2M and Zr_3M phases are shown fixed, and relative to them, the free energy of the glass or supercooled liquid is shown for three temperatures. The free energy minimum for the IQ and DoQ phases is shown rather broad, considering that the solubility limit may be high for formation over a wide composition range. Arrows 1 and 2 represent the heating-induced partial and full crystallization reactions of glass → [glass' + IQ] and [glass' + IQ] → [ZrM + Zr_4M_3 + Zr_2M + Zr_3M], respectively, while arrows 3 and 4 represent the rolling-induced transformations of glass → [glass' + IQ + DQ] and glass → [glass' + IQ + DoQ + APC], respectively. On annealing at quasi-crystallization onset (~750 K),

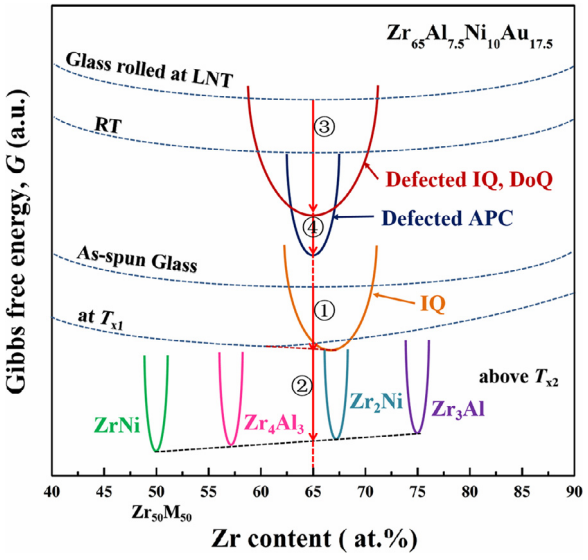

Fig. 8. The relative free energies of the phases relevant for the transformations on cold-rolling a melt-spun ribbon of $Zr_{65}Al_{7.5}Ni_{10}Au_{17.5}$ glass. In this schematic figure, the alloy is treated as a binary (Zr + solute) system. Arrows 1 and 2 show the heating-induced first crystallization of glass → [glass' + IQ] and the second crystallization of [glass' + IQ] → [Zr_2M + Zr_4Al_3 + Zr_3Al + ZrM}, respectively. Arrows 3 and 4 correspond to the rolling-induced transformation of glass → [glass' + IQ + DoQ] and glass → [glass'' + IQ + DoQ + APQ], respectively.

the glass can lower its free energy (arrow 1 in this figure) by undergoing primary quasi-crystallization to the IQ. At this temperature, polymorphic crystallization to IQ would not be possible thermodynamically (the free energy would rise) or kinetically (partition would occur). At RT or LNT, however, the driving force for quasi-crystallization is much greater, and polymorphic quasi-crystallization to IQ (arrow 2) is possible. Furthermore, solute transport is inhibited, so the formation of the Zr_2M compound with composition different from that of the glass is impossible. Suppression of equilibrium compound formation is important to avoid embrittlement on annealing. Polymorphic quasi-crystallization has also been reported on continuous heating for Pd-U-Si [26,27], Al-Cu-V [28] and Al-Mn-Si [29] amorphous ribbons, accompanying a distinct exotherm. However, the quasi-crystallized ribbons are very brittle, in marked contrast to the good plasticity for the cold-rolled ribbons in which the formation of the IQ and DoQ phases is by polymorphic crystallization.

The IQ and DoQ phases do not have a periodic translational lattice and hence cannot have plastic deformability via the glide of dislocations at RT [40,41]. Previous studies of mechanical properties [11,40,41] have reported that IQ-based alloys can be deformed plastically at high temperatures through the climb of dislocations via thermal diffusion. These results also suggest that IQ-based alloys can show plastic deformability, even at RT, through higher atomic mobility associated with incomplete long-range icosahedral order, typically associated with a high density of internal defects and pronounced distortions. Incomplete IQ, DoQ and APC order may permit plastic deformation via fast atomic rearrangements. In addition, considering that plastic glass ribbons containing large size IQ, DoQ and APC particles are obtained only for $Zr_{65}Al_{7.5}Ni_{10}Cu_{17.5-x}Au_x$ alloys, the fast rearrangements under an applied stress may be associated with repulsive Au-Ni bonding [42].

5. Conclusions

Cold-rolling of initially fully glassy $Zr_{65}Al_{7.5}Ni_{10}Cu_{17.5-x}Au_x$ (x = 6–17.5 at%) ribbons induces formation of IQ phase at 6–15 at% Au and [IQ + DoQ + APC] phases at 17.5 at% Au. After rolling to $R \approx 70\%$, the volume fractions of these phases reach about 20 % in the residual glassy matrix. The particle diameters of the IQ and DoQ phases are 50–100 nm and 150–200 nm, respectively. The IQ- and [IQ + DoQ + APC]-based alloys have good cold-rollability to ~70% and can be bent through 180°, and back, without breaking. A number of slip markings are observed on the outer bent surface. This bending plasticity is contrast to the extremely brittle nature of the corresponding annealed alloys consisting of nanoscale IQ (10–15 nm diameter) particles in the residual glassy matrix. The H_V of the 10Au and 15Au ribbons is about 520 for the as-spun glass, decreases with increasing reduction in thickness and reaches as low as about 430 and 395, respectively, at R = 70%. The IQ-based ribbon exhibits some serrated flow under tensile load, even in the nominally elastic region, presumably due to local slip at rolling-induced shear-band sites. The formation of [IQ + glass'] and [IQ + DoQ + APC + glass'] alloys by cold-rolling is facilitated by the nucleation sites and higher growth rates of IQ, DoQ and APC phases at shear bands. The HRTEM images reveal high densities of defects and significant distortions, and the lack of long-range quasiperiodic atomic configurations. The formation of an incompletely ordered IQ atomic configuration is presumed to be the origin for the good plasticity for the glass alloys containing large size IQ- and [IQ + DoQ + APC] particles. This first success of synthesizing [IQ + glass'] and [IQ + DoQ + APC + glass'] alloys with good plasticity is promising for the future development of such materials for structural and functional applications.

Declaration of Competing Interest

None.

Acknowledgments

The authors are grateful for support from the Recruitment Program of Global Experts “1000 Talents Plan” (WQ20121200052), the National Natural Science Foundation of China (51771131), the Program for High-Level Entrepreneurial and Innovative Talents Group in Jiangsu Province; the Fundamental Research Funds for the Central Universities (Grant 2017XKQY009), the Deanship of Scientific Research (DSR), King Abdulaziz University, Jeddah, Saudi Arabia (1-1-435/HiCi), and the Ministry of Education and Science of the Russian Federation in the framework of the program aimed to increase the competitiveness of the National University of Science and Technology, “MISiS” (No. K2-2019-002). ALG acknowledges support from the European Research Council under the European Union’s Horizon 2020 Research and Innovation program (grant ERC-2015-AdG-695487: Extend Glass).

References

[1] W. Klement, R.H. Willens, P. Duwez, Non-crystalline structure in solidified gold-silicon alloys, Nature 187 (1960) 869–870.
[2] D. Shechtman, I. Blech, D. Gratias, J.W. Cahn, Metallic phase with long-range orientational order and no translational symmetry, Phys. Rev. Lett. 53 (1984) 1951–1953.
[3] A. Inoue, High strength bulk amorphous alloys with low critical cooling rates, Mater. Trans., JIM 36 (1995) 866–875.
[4] A.L. Greer, E. Ma, bulk metallic glasses: At the cutting edge of metals research, MRS Bull. (2007) 611–619.
[5] W.L. Johnson, Bulk glass-forming metallic alloys: Science and technology, MRS Bull. 24 (1999) 42–56.
[6] A. Inoue, Stabilization of metallic supercooled liquid and bulk amorphous alloys, Acta Mater 48 (2000) 279–306.
[7] C. Suryanarayana, A. Inoue, Bulk Metallic Glasses, 2nd Edn, CRC Press, Boca Raton, FL, 2017.
[8] A. Inoue, A. Takeuchi, Recent development and application products of bulk glassy alloys, Acta Mater 59 (2011) 2243–2267.
[9] T. Masumoto, A. Inoue, M. Oguchi, K. Fukamichi, K. Hiraga, M. Hirabayashi, Structural, thermal and electrical properties of Al-Mn quasicrystals obtained by melt quenching, Trans. JIM 27 (1986) 81–86.

[10] Y. Yokoyama, A. Inoue, T. Masumoto, Mechanical properties, fracture mode and deformation behavior of $Al_{70}Pd_{20}Mn_{10}$ single-quasicrystal, Mater. Trans, JIM 34 (1993) 135–145.
[11] A.P. Tsai, H. Suenaga, M. Ohmori, Y. Yokoyama, A. Inoue, T. Masumoto, Temperature dependence of hardness and expansion in an icosahedral Al-Pd-Mn alloy, Jpn. J. Appl. Phys. 31 (1992) 2530–2531.
[12] H.T. Ren, J. Pan, Q. Chen, K.C. Chan, Y. Liu, L. Liu, Enhancement of plasticity and toughness in monolithic Zr-based bulk metallic glass by heterogeneous microstructure, Scripta Mater 64 (2011) 609–612.
[13] A.D. Setyawan, J. Saida, H. Kato, M. Matsushita, A. Inoue, Deformation-induced structural transformation leading to compressive plasticity in $Zr_{65}Al_{7.5}Ni_{10}Cu_{12.5}M_5$ (M=Nb,Pd) glassy alloys, J. Mater. Res. 25 (2010) 1149–1158.
[14] Z.W. Zhu, L. Gu, G.Q. Xie, W. Zhang, A. Inoue, H.F. Zhang, Z.Q. Hu, Relation between icosahedral short-range ordering and plastic deformation in Zr-Nb-Cu-Ni-Al bulk metallic glasses, Acta Mater 59 (2011) 2814–2822.
[15] A. Inoue, T. Zhang, J. Saida, M. Matsushita, M.W. Chen, T. Sakurai, Formation of icosahedral quasicrystalline phase in Zr-Al-Ni-Cu-M (M=Ag, Pd, Au or Pt) systems, Mater. Trans. JIM 40 (1999) 1181–1184.
[16] M.W. Chen, A. Inoue, T. Zhang, A. Sakai, T. Sakurai, Quasicrystals and nano-quasicrystals in annealed ZrAlNiCuAg metallic glasses, Intermetallics 8 (2000) 493–498.
[17] J. Saida, M. Matsushita, C. Li, A. Inoue, Effects of Ag and Pd on the nucleation and growth of the nano-icosahedral phase in $Zr_{65}Al_{7.5}Ni_{10}Cu_{7.5}M_{10}$ (M = Ag or Pd) metallic glasses, Phil. Mag. Lett. 80 (2000) 737–743.
[18] M.M. Li, A. Inoue, Y. Han, F.L. Kong, S.L. Zhu, E. Shalaan, F. Al-Marzouki, Influence of Ag replacement on supercooled liquid region and icosahedral phase precipitation of $Zr_{65}Al_{7.5}Ni_{10}Cu_{17.5-x}Ag_x$ (x = 0–17.5 at%) glassy alloys, J. Alloy Comp. 735 (2018) 1712–1721.
[19] T. Yamazaki, M. Yamada, K. Fujita, H. Kato, D.H. Kim, Effects of noble metal addition on plastic deformation of Zr-Cu-Ni-Al based bulk metallic glasses, J. Jpn. Soc. Powder Metall. 63 (2016) 230–238.
[20] M. Yamada, R. Kamisato, T. Yamazaki, H. Adachi, K. Tsuchiya, Y. Yokoyama, Nanocrystallization of Zr-Cu-Ni-Al-Au glassy alloys during severe plastic deformation, IOP Conf. Series: Mater. Sci. Eng. 63 (2014) 012167.
[21] H.W. Bi, A. Inoue, F.F. Han, Y. Han, F.L. Kong, S.L. Zhu, E. Shalaan, F. Al-Marzouki, A.L. Greer, Novel deformation-induced polymorphic crystallization and softening of Al-based amorphous alloys, Acta Mater 147 (2018) 90–99.
[22] H.M. Kimura, A. Inoue, Y. Bizen, T. Masumoto, H.S. Chen, New quasi-crystalline and amorphous phases in rapidly quenched Al-Ge-(Cr, Mn) and Al-Si-(Cr, Mn) alloys with high metalloid concentrations, Mater. Sci. Eng. 99 (1988) 449–452.
[23] Y. Kim, A. Inoue, T. Masumoto, Ultrahigh tensile strength of $Al_{88}Y_2Ni_9M_1$ (M = Mn or Fe) amorphous alloys containing finely dispersed fcc-Al particles, Mater. Trans. JIM 31 (1990) 747–749.
[24] Y.H. Kim, K. Hiraga, A. Inoue, T. Masumoto, H.H. Jo, Crystallization and high mechanical strength of Al-based amorphous alloys, Mater. Trans. JIM 35 (1994) 293–302.
[25] A. Inoue, Amorphous, nanoquasicrystalline and nanocrystalline alloys in Al-based systems, Prog. Mater. Sci. 43 (1998) 365–520.
[26] S.J. Poon, A.J. Drehman, K.R. Lawless, Glassy to icosahedral phase transformation in Pd-U-Si alloys, Phys. Rev. Lett. 55 (1985) 2324–2327.
[27] B.-Z. Feng, Y. Cheng, J.-D. Kang, The effect of adding Al on $Pd_{80}Si_{20}$ metallic glass, J. Non-Cryst. Solids 119 (1990) 181–186.
[28] J.C. Holzer, K.F. Kelton, Kinetics of the amorphous to icosahedral phase transformation in Al-Cu-V alloys, Acta Metall. Mater. 39 (1991) 1833–1843.
[29] K. Hiraga, D. Shindo, High-resolution electron microscopy and atomic arrangements of Al–Mn–Si and Al–Li–Cu icosahedral quasicrystals, Mater. Trans. JIM 31 (1990) 567–572.
[30] D.B. Williams, C.B. Carter, in: Transmission Electron Microscopy: A Textbook for Materials Science, Diffraction, 2nd ed., Springer, Boston, MA, 2009, p. 11.
[31] H. Chen, D.X. Li, K.H. Kuo, New type of two-dimensional quasicrystal with twelvefold rotational symmetry, Phys. Rev. Lett. 60 (1988) 1645–1648.
[32] J. Reyes-Gasga, R. Hernández, M. José-Yacamán, A twelve-fold quasicrystalline phase in Bi-Mn alloys, Scr. Metall. Mater. 25 (1991) 323–330.
[33] M. Uchida, S. Horiuchi, Twelve-fold quasicrystal and its approximant of $Ta_{62}Te_{38}$ interpreted as modulated crystals, Micron 31 (2000) 493–497.
[34] D.K. Misra, R.S. Tiwari, O.N. Srivastava, Effect of Fe substitution on the stabilization of the icosahedral phase in Al-Cu-V alloys, Cryst. Res. Technol. 36 (2001) 419–427.
[35] A. Singh, S. Ranganathan, L. Bendersky, Quasicrystalline phases and their approximants in AlMnZn alloys, Acta Mater 45 (1997) 5327–5336.
[36] M.Q. Jiang, L.H. Dai, On the origin of shear banding instability in metallic glasses, J. Mech. Phys. Solids 57 (2009) 1267–1292.
[37] Y.Q. Cheng, Z. Han, Y. Li, E. Ma, Cold versus hot shear banding in bulk metallic glass, Phys. Rev. B 80 (2009) 134115.
[38] A.L. Greer, Y.Q. Cheng, E. Ma, Shear bands in metallic glasses, Mater. Sci. Eng. R 74 (2013) 71–132.
[39] J.J. Lewandowski, A.L. Greer, Temperature rise at shear bands in metallic glasses, Nat. Mater. 5 (2006) 15–18.
[40] Z. Zhang, M. Wollgarten, K. Urban, Analysis of dislocations in icosahedral Al–Cu–Fe alloy by transmission electron microscopy, Philos. Mag. Lett. 61 (1990) 125–131.
[41] A. Inoue, Y. Yokoyama, T. Masumoto, Mechanical properties and deformation behavior of large $Al_{70}Pd_{20}Mn_{10}$ single quasi-crystals, Mater. Sci. Eng. A 181210 (182) (1994) 850–855.
[42] A. Takeuchi, A. Inoue, Classification of bulk metallic glasses by atomic size difference, heat of mixing and period of constituent elements and its application to characterization of the main alloying element, Mater. Trans. 46 (2005) 2817–2829.